Published manuscript at https://doi.org/10.1016/j.cmpb.2022.106912

# Patient-specific multi-scale design optimization of transcatheter aortic valve stents

Sara Barati[a], Nasser Fatouraee[a], Malikeh Nabaei[a], Lorenza Petrini[c], Francesco Migliavacca[b], Giulia Luraghi[b], Josè Felix Rodriguez Matas[b]

a. Biological Fluid Dynamics Research Laboratory, Biomedical Engineering Department, Amirkabir University of Technology, 350 Hafez Ave, Tehran, Iran

b. Laboratory of Biological Structure Mechanics (LaBS), Department of Chemistry, Materials, and Chemical Engineering "Giulio Natta", Politecnico di Milano, Piazza Leonardo da Vinci 32, 20133 Milan, Italy

c. Department of Civil and Environmental Engineering, Politecnico di Milano, Piazza Leonardo da Vinci 32, 20133 Milan, Italy

Keywords: Transcatheter aortic valve; Stent; Finite element method; Multi-objective optimization; Gaussian process regression models

**Corresponding Authors:**

1. **Nasser Fatouraee**, Associate professor
   Address: Biological Fluid Dynamics Research Laboratory, Biomedical Engineering Department, Amirkabir University of Technology, 350 Hafez Ave, Tehran, Iran
   Tel: +9866468186
   E-mail: nasser@aut.ac.ir
2. **Josè Felix Rodriguez Matas**, Associate professor
   Address: Laboratory of Biological Structure Mechanics (LaBS), Department of Chemistry, Materials, and Chemical Engineering "Giulio Natta", Politecnico di Milano, Piazza Leonardo da Vinci 32, 20133 Milan, Italy
   Tel: +390223993209
   E-mail: josefelix.rodriguezmatas@polimi.it
3. **Giulia Luraghi**, Researcher TD
   Address: Laboratory of Biological Structure Mechanics (LaBS), Department of Chemistry, Materials, and Chemical Engineering "Giulio Natta", Politecnico di Milano, Piazza Leonardo da Vinci 32, 20133 Milan, Italy
   Tel: +39 02 2399 3399
   E-mail: giulia.luraghi@polimi.it

Published manuscript at https://doi.org/10.1016/j.cmpb.2022.106912

## Abstract

***Background and Objective*:** Transcatheter aortic valve implantation (TAVI) has become the standard treatment for a wide range of patients with aortic stenosis. Although some of the TAVI post-operative complications are addressed in newer designs, other complications and lack of long-term and durability data on the performance of these prostheses are limiting this procedure from becoming the standard for heart valve replacements. The design optimization of these devices with the finite element and optimization techniques can help increase their performance quality and reduce the risk of malfunctioning. Most performance metrics of these prostheses are morphology-dependent, and the design and the selection of the device before implantation should be planned for each individual patient.

***Methods*:** In this study, a patient-specific aortic root geometry was utilized for the crimping and implantation simulation of 50 stent samples. The results of simulations were then evaluated and used for developing regression models. The strut width and thickness, the number of cells and patterns, the size of stent cells, and the diameter profile of the stent were optimized with two sets of optimization processes. The objective functions included the maximum crimping strain, radial strength, anchorage area, and the eccentricity of the stent.

***Results*:** The optimization process was successful in finding optimal models with up to 40% decrease in the maximum crimping strain, 261% increase in the radial strength, 67% reduction in the eccentricity, and about an eightfold increase in the anchorage area compared to the reference device.

***Conclusions*:** The stents with larger distal diameters perform better in the selected objective functions. They provide better anchorage in the aortic root resulting in a smaller gap between the device and the surrounding tissue and smaller contact pressure. This framework can be used in designing patient-specific stents and improving the performance of these devices and the outcome of the implantation process.

**Keywords**: Transcatheter aortic valve; Stent; Finite element method; Multi-objective optimization; Gaussian process regression models

Published manuscript at https://doi.org/10.1016/j.cmpb.2022.106912

# 1 Introduction

Transcatheter aortic valve implantation (TAVI) is a well-established procedure for the treatment of high and intermediate-risk patients with aortic valve stenosis [1]. This procedure has been evaluated for lower-risk patients with severe aortic stenosis and proven non-inferior compared to the standard surgical aortic valve replacement [2]. These devices have been associated with some complications, and new models are developed to overcome the limitations of their use [3–5]. The main complications of these devices are post-implantation paravalvular leakage [6] and conduction abnormalities leading to permanent pacemaker implantation [7]. Clinical trials show that improving prosthetic valve design reduces the post-intervention risk of complications [8].

The results of in-silico studies demonstrate the reliability of finite element simulations in predicting the outcome of TAVI in patients. The simulation studies of the TAVI procedure can be divided in four groups: i) finite element structural simulations, ii) computational fluid dynamics simulations, iii) fluid-structure interaction simulations, and iv) optimization studies. The structural simulations explore the mechanical performance of the device in crimping and releasing, implantation position and depth [9], device anchorage [10], interaction with the arterial wall [11], and the gaps associated with the paravalvular leakage [12,13]. The computational fluid dynamic simulations are utilized for evaluating the device's hemodynamic performance and the degree of paravalvular leakage [10,14]. The fluid-structure interaction simulations are used to evaluate the device's performance when considering the heart cycle [15,16] and the prosthetic valve hemodynamics [17]. The optimization studies aim at improving the current designs for better performance and reducing post-intervention complications [18–21]. In a recent study, Carbonaro et al. [20] proposed a multi-objective optimization framework for the strut cross-section and the overall shape of the stent. In their work, three objective functions, the pullout force, maximum contact pressure, and the maximum stress exerted on the aortic wall, were optimized in idealized aortic root geometries for healthy and diseased scenarios.

In our previous study [21], we proposed a cost-effective optimization framework for structural optimization of stents regarding six design parameters; strut width and thickness, number of cells and patterns, and the height of the first and second stent cells. The framework can be applied to any stent shape and material properties to design

structurally optimized devices. However, the comprehensive optimization of TAVI stents should include both structural and functional optimization of the device since the majority of functional metrics of the TAVI stents are morphology-dependent [9,22–24]. This necessitates the patient-specific optimization of these devices for better-individualized applicability of them.

In this study, a multi-scale optimization framework exploiting patient-specific data was applied to the stent for TAVI, aiming to improve its performance. The TAVI stents are structurally optimized with the Genetic Algorithm (GA) optimization framework presented in our previous study [21]. A multi-objective optimization problem is used to account for different performance metrics. Some optimal designs from the Pareto surface are then chosen and implanted in the patient-specific geometry. The performance of the optimized devices is compared against those obtained with a reference device implanted in the same patient-specific geometry. The ultimate goal of this study is to provide a framework to help the interventional cardiologists choosing, among available devices, the best option for patients undergoing TAVI and minimize the post-procedural complications. Moreover, the proposed methodology, applied to a large number of patient-specific cases, can be used by the manufacturing companies to investigate the necessity of modifying the characteristics of a particular device design.

## 2 Methods

The framework presented in this paper regarding the optimization of a TAVI stent consists of the following steps: 1) creation of the FE model of a patient-specific aortic root, including the calcified deposit and native aortic valve; 2) parametrization of the stent geometry and selection of the design parameters, following a sensitivity analysis to identify the most important ones; 3) definition of the optimization problem regarding the performance metrics of the TAVI stent; 4) solution of the optimization problem to determine the optimal designs, and 5) comparing the optimal design with a reference stent based on the defined performance metrics. Each of these steps is described in the following sections.

## 2.1 Model set-up

### 2.1.1 Aortic root geometry and material

A patient-specific aortic root geometry reconstructed as described in [15] was used to implant the stent and evaluate the functional aspects of the TAVI. The geometry corresponded to the end-diastolic phase of the cardiac cycle and comprised the aortic root, a portion of ascending aorta, the native aortic valves, and calcification deposits. The aortic annulus diameter was 23mm, which is in the range of candidates for the Evolut R device of size 26 [25]. In the patient-specific model, the calcified deposits were similar to a general aortic valve calcification pattern (coaptation pattern) [17,26].

An isotropic hyperelastic material with a Yeoh constitutive formulation was employed to describe the mechanical behavior of the aortic root wall [27]:

$$W = C_{10}(\bar{I}_1 \quad 3) + C_{20}(\bar{I}_1 \quad 3)^2, \tag{1}$$

where $\bar{I}_1$ is the first invariant of the isochoric part of the left Cauchy-Green tensor and $C_{10}$ and $C_{20}$ are equal to 0.015 MPa and 0.158 MPa, respectively, with density and Poisson ratio of 1100 kg/m$^3$ and 0.49. The native valves were modeled using an incompressible generalized Mooney-Rivlin hyperelastic model with a density of 1100 kg/m$^3$ and a Poisson ratio of 0.49 [28]:

$$W = C_{10}(\bar{I}_1 \quad 3) + C_{01}(\bar{I}_2 \quad 3) + C_{11}(\bar{I}_1 \quad 3)(\bar{I}_2 \quad 2), \tag{2}$$

where $C_{10}$ =32.823e-3 MPa, $C_{01}$ =2.955e-3 MPa and $C_{11}$ =585.79e-3 MPa. An isotropic linear elastic material was adopted for the calcified deposit with a density of 2000 kg/m3, elastic modulus of 12.6 MPa, and a Poisson ratio of 0.45 [15].

A mesh sensitivity analysis was performed regarding maximum principal stress in the patient-specific model components. The aorta was discretized with 94242 fully integrated hexahedral elements. The native leaflets were meshed with 1957 quadrilateral shell elements with reduced integration formulation and hourglass control. A uniform thickness of 0.5 mm was set for the leaflets. The calcification deposits were meshed with 35655 linear tetrahedral elements. A surface-to-surface tie constraint between native leaflets and the calcific deposits and a node-to-surface tie constraint was set between the leaflets' external edges and aortic root internal wall [15].

Published manuscript at https://doi.org/10.1016/j.cmpb.2022.106912

### 2.1.2 Stent geometric model and material

To generate the 3D model of TAVI frames, a planar sketch was first created with the computer-aided design software SolidWorks (Dassault Systèmes SolidWorks Corp., Waltham, MA). The planar sketch has been parametrized in terms of the following geometric parameters (see Fig. 1a-d): i) the number of cells, $c$; ii) the number of patterns, $p$; iii) the strut width, $w$; iv) the strut thickness, $t$; v) the height of the first cell, $L_1$; vi) the height of the middle cells, $L_2$ (assumed equal for all middle cells of the stent); and vii) the height of the stent, $H$. A MATLAB (MathWorks, Inc., MA, USA) code was used to wrap the planar sketch using the stent diameter profile shown in Fig. 1c.

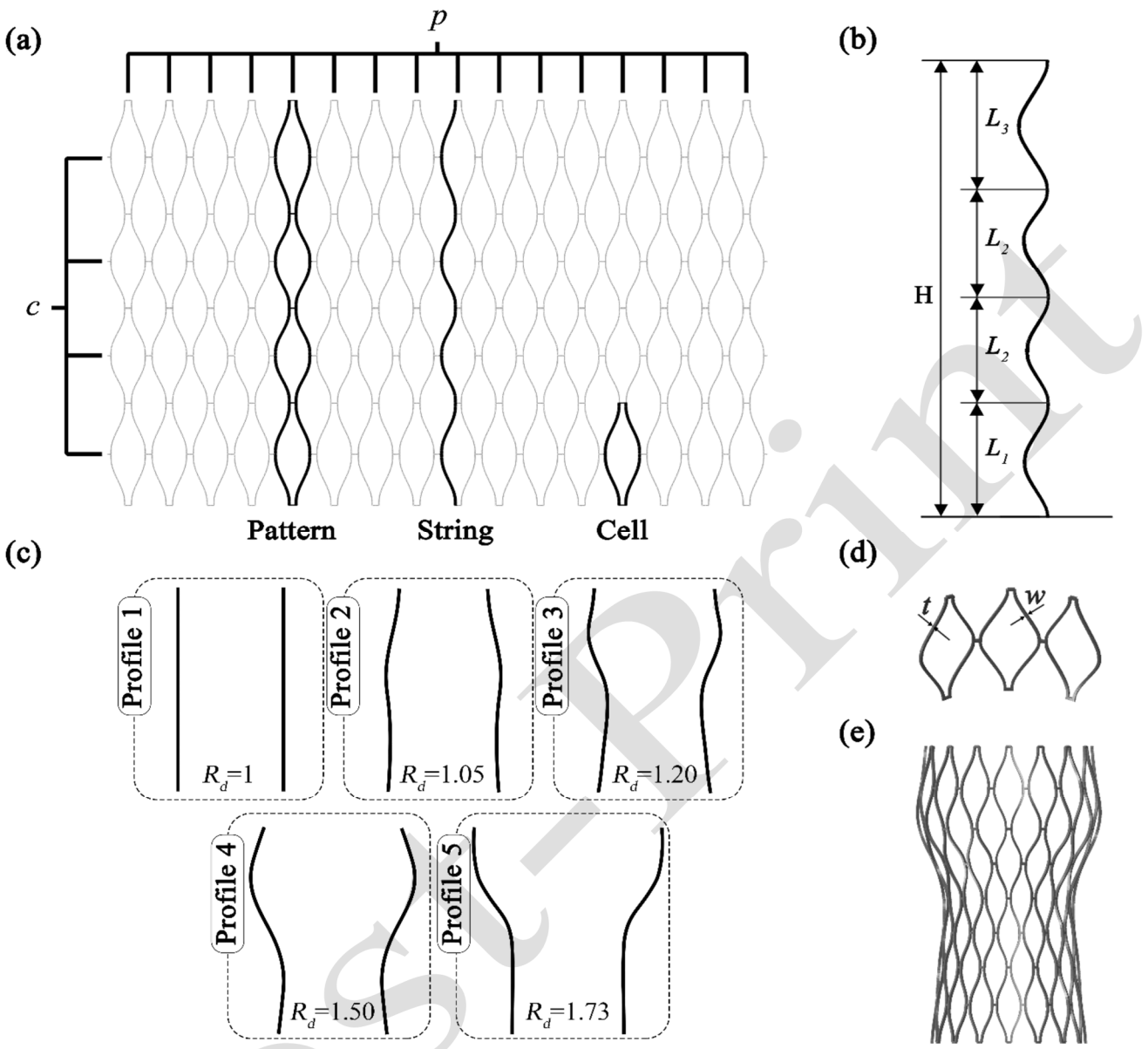


**Fig. 1.** a) The geometric parametrization. Parameters $p$ (number of patterns) and $c$ (number of cells) are shown on the planar sketch of the stent, b) Parameters $L_1$ and $L_2$ represent the first and middle cell heights, c) Diameter profiles. The diameter ratio ($R_d$) of each profile is the maximum to proximal diameter ratio of the stent, with the proximal diameter assumed equal to 26 mm for all diameter profiles. d) The width ($w$) and thickness ($t$) of the struts. e) The final configuration of the stent created with parameters: $c$=4, $p$=16, $w$=0.35 mm, $t$=0.3 mm and $R_d$=1.20 (Profile 3).

Five diameter profiles corresponding to a cylinder and four commercially available TAVI stents (see Fig. 1c) have been considered to study the effect of the diameter profile on the frame's performance metrics. These diameter profiles can be characterized by the maximum to the proximal diameter ratio, $R_d$, of the stent (Fig. 1c), where the proximal diameter has been assumed the same for all the stents and equal to $D_p$ =26 mm. The five considered profiles correspond to: Profile 1 ($R_d = 1.0$), Profile 2 ($R_d = 1.05$), Profile 3 ($R_d = 1.20$), Profile 4

($R_d = 1.50$), and Profile 5 ($R_d = 1.73$). Also, the device's height was considered fixed ($H$=50mm) for all models. The upper and lower bounds of the design parameters were chosen based on the data from the literature [18–20,29] such that it resulted in valid geometries without overlapping struts (Table 1).

**Table 1** Geometric parameters, their corresponding lower and upper bounds and levels for the Design of Experiments (DoE)

| Parameter | Lower Bound | Upper Bound |
|---|---|---|
| Number of cells, *c* | 3 | 5 |
| Number of pattern repetitions, *p* | 9 | 15 |
| Strut thickness, *t* (mm) | 0.3 | 0.5 |
| Strut width, *w* (mm) | 0.2 | 0.5 |

The performance of the optimized device was compared against a reference device with characteristics given in Table 2.

**Table 2** Geometric parameters of the implanted stent

| Parameter | Value |
|---|---|
| Number of cells, *c* | 5 |
| Number of pattern repetitions, *p* | 15 |
| Strut thickness, *t* (mm) | 0.2 |
| Strut width, *w* (mm) | 0.3 |
| Proximal diameter (mm) | 26 |
| $R_d$ | 1.2 |

All frames were self-expandable stents made of Ni-Ti alloy, with the superelastic constitutive model proposed by Auricchio and Taylor (1997) used to simulate the mechanical behavior of the stents. Table 3 provides the mechanical properties of the Ni-Ti alloy used in the simulation of the models [30].

**Table 3** Ni-Ti Alloy material properties

| Parameter | Value |
|---|---|
| Austenite Elasticity (MPa) | 45000 |
| Austenite Poisson's Ratio | 0.3 |
| Martensite Elasticity (MPa) | 22500 |
| Martensite Poisson's Ratio | 0.3 |
| Transformation Strain | 0.0426 |
| Start of Transformation Loading (MPa) | 310 |
| End of Transformation Loading (MPa) | 335 |
| Reference Temperature (°C) | 37 |
| Start of Transformation Unloading (MPa) | 100 |
| End of Transformation Unloading (MPa) | 75 |

Stents were meshed with quadratic beam elements. A mesh sensitivity analysis was performed in terms of the maximum crimping strain, resulting in an average element size of 0.5 mm. The mesh characteristics were kept the same for all models. Choosing the appropriate mesh was guided by maintaining a balance between

computational cost and accuracy of simulations. Depending on the stent design parameters, the number of beam elements in the stent varied between 2300 to 4021 (Fig. 2c).

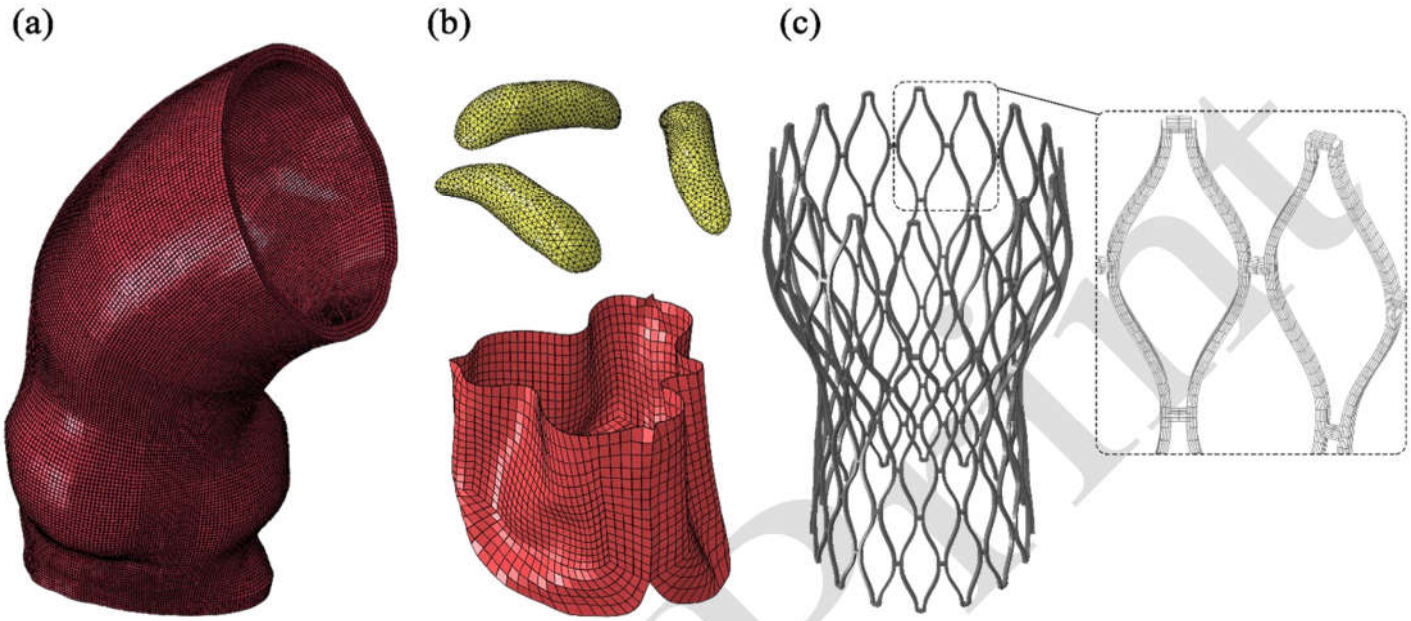


**Fig. 2.** Discretization of the model components. a) Aortic root, b) Native leaflets and calcification deposits, c) TAVI stent, the inset shows a rendering of the quadratic beam elements showing the 25 Gauss points used to integrate the element cross-section.

The prosthetic leaflets were neglected in the simulations because the effect of the leaflets on the stent's structural performance is negligible [31].

### 2.1.3 Finite Element simulations

Implantation of the TAVI in the patient-specific aortic root was simulated in two steps: 1) Crimping step, where the stent is crimped and inserted into the catheter, and 2) Release step, where the stent is released from the catheter and left to expand in the implantation site.

**Crimping step.** The crimping process of the stent was performed by applying a radial displacement to 12 parallel planes until a final diameter of 8mm (Fig. 3b). Frictionless self-contact between the stent struts and a hard contact between the stent and the rigid planes were defined. Symmetry boundary conditions were applied on the nodes at the proximal end of the stent, whereas the distal end was left free to allow for stent elongation.

Published manuscript at https://doi.org/10.1016/j.cmpb.2022.106912

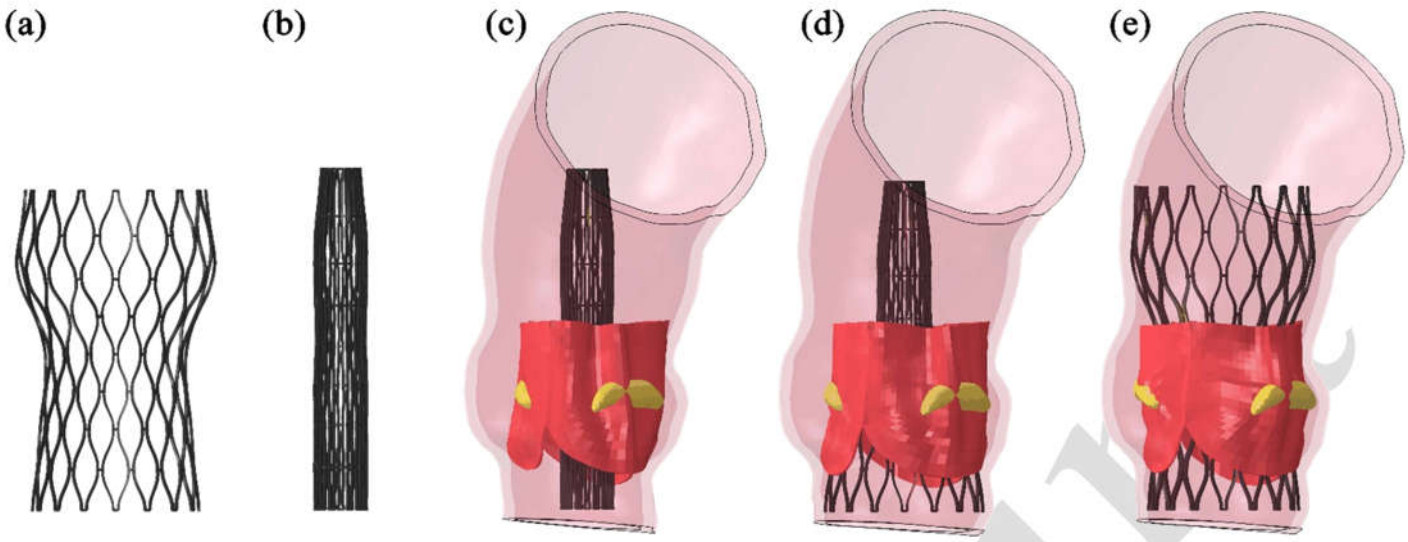


**Fig. 3.** TAVI simulation steps; a) stent initial configuration, b) end of crimping step, c) aligning the crimped stent in the aortic root, d) stent expansion from the proximal end, e) final implanted configuration of the stent in the aortic root

**Release step.** The patient-specific model of the aortic root was prepared for implantation by radial expansion with a rigid catheter up to a diameter of 10 mm [15]. To perform the stent deployment simulation, the stent was positioned in the midway implantation depth (about 4 millimeters below the annulus) [16,32] and aligned with the aortic valve (Fig. 3c). An axial displacement was applied on the reference points of the parallel planes towards the ascending aorta, releasing the stent from the proximal end toward the distal end to allow the stent to expand in the aortic root (Fig. 3d-e). A friction coefficient of 0.1 [33] between the stent and the aorta, the leaflets, and the calcification deposits were considered in this step. The proximal and distal ends of the aortic root were constrained to move only in the radial direction of their respective planes. A resting phase followed the release step to ensure the complete expansion and anchoring of the device in the implantation site.

The simulations were performed using the Abaqus explicit solver (Dassault Systèmes Simulia Corp., Providence, RI, USA) on a system featuring 32 CPUs (Intel Xeon64) and 250 GB of RAM. The mass scaling was set to target a minimum time increment of $10^{-6}$ s to minimize the dynamic effects. Besides a mass proportional Rayleigh damping of $\alpha = 100\ s^{-1}$ for the stent, aortic root and calcification deposits and $\alpha = 1000\ s^{-1}$ for native leaflets were set. For this combination of parameters, the kinetic energy was less than 5% of the internal energy during the entire simulation, respecting the quasi-static deformation assumption.

## 2.2 Performance of TAVI stent

The optimization of the TAVI stent frame involves structural and functional performance aspects. The quality of structural performance of the stent during crimping and expansion can be evaluated by the maximum crimping strain and the radial strength of the stent. Regarding functional performance, the risk of migration is measured by the contact area between the stent and the aortic root. In addition, the maximum contact pressure exerted by the stent on the aortic root is an indicator of possible tissue damage resulting from the implantation. Conduction abnormalities have been proven to be related to the maximum contact pressure in the left ventricular outflow tract ( LVOT) under the area between non-coronary cusp (NCC) and right coronary cusp (RCC) [19]. Other metrics, such as eccentricity and the gap area between the stent and the aortic root are also associated with paravalvular leakage and can be calculated for evaluating valve performance [34]. In this study, a total of four metrics have been used to assess the performance of the TAVI stent. The structural performance of the stent has been evaluated by the maximum crimping strain and radial strength in crimping. On the contrary, the quality of the functional performance has been evaluated through the anchorage area and the eccentricity post-implantation. Each of these performance metrics is defined in the following.

**Maximum Crimping Strain (MCS).** The fatigue life of the Ni-Ti alloy stents depends mainly on the maximum strain reached during their application [35]. Hence, the maximum strain occurring during the crimping of the stent into the catheter was minimized. Further, to avoid the stent material exceeding the material yielding strain [36], the maximum acceptable strain was set to be strictly less than 0.1.

$$MCS_{max} < 0.1 \tag{3}$$

**Radial Strength (RS).** According to ASTM-F3067-14, the maximum radial force is equivalent to the radial strength of the stent [37,38]. The radial force-diameter curve and the radial strength were evaluated for each model. Higher radial strength contributes to the better ability of the stent for opening highly calcified aortic valves and better anchorage. On the contrary, excessive amounts of radial force can cause tissue damage and increase the probability of conduction abnormalities [11,12].

$$RS_{max} = Max\ (Radial\ Force) \tag{4}$$

**Anchorage Area (AA).** To evaluate the quality of stent anchorage in the aortic root, the contact area between the stent and the aortic root was measured [16]. A higher contact area represents better anchorage and reduces the probability of stent migration [39]. The contact area measured in this regard is the area of the stent elements that are in contact with the aortic root (Fig. 4).

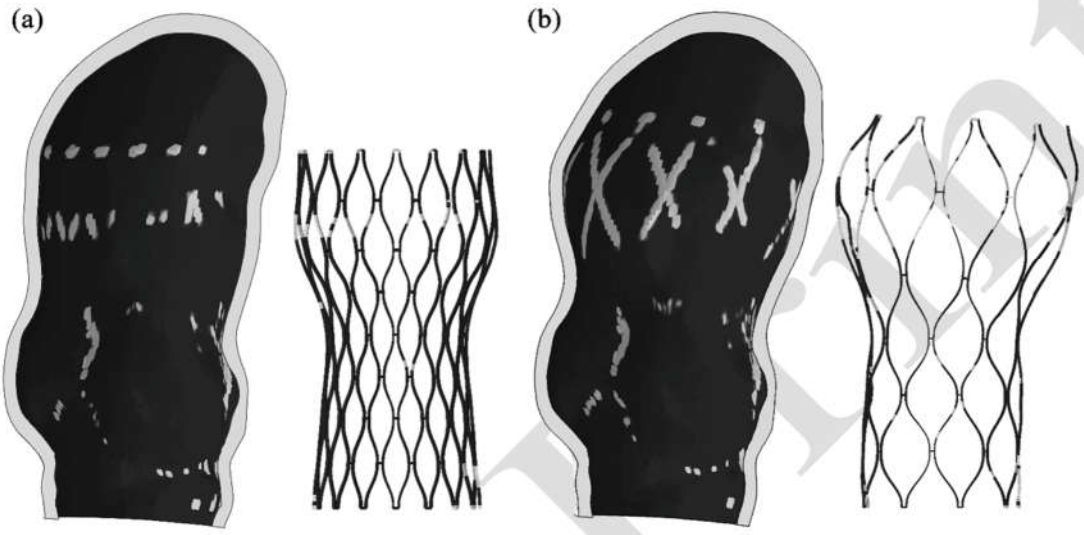


**Fig. 4.** The contact regions on a portion of the aortic root and the stent at the end of implantation simulation for two cases with diameter ratios of 1.20 (a) and 1.73 (b). The light gray regions on the aortic root and the stent mark the elements with contact pressure higher than zero. The traces of the stent struts on the aortic wall are visible, especially in the proximal and distal regions of the aortic root. The contact regions in the middle part of the aorta (between the annulus and sino-tubular junction) include both the stent and native leaflets' contact traces.

**Eccentricity (E).** Post-deployment stent deformation was evaluated by measuring the stent eccentricity, which quantifies the elliptic shape of the stent frame at the annulus level. Studies show that higher eccentricity might lead to malfunction of the valve [9,34]; hence, this objective was set to be minimized in the optimization process.

$$E = 1 \quad \left(\frac{Stent\ diameter_{min}^{Annulus}}{Stent\ diameter_{max}^{Annulus}}\right) \tag{5}$$

## 2.3 Optimization

The optimization follows the flowchart in Fig. 5. First, we define a three-level full factorial experiment for the four design variables $c$, $p$, $t$, and $w$ (see Table 2) for each diameter profile (treated as a categorical variable), defining a total of 405 samples. For each sample, the value of $L_1$and $L_2$ were optimized using a surrogate model for the stent crimping defined in [21] such that the maximum strain in the stent during crimping is minimum. In a second step, with the optimized $L_1$and $L_2$, for each combination of design variables $c$, $p$, $t$, $w$, and $R_d$, 50

combinations out of the 405 possible were randomly selected, and 3D TAVI stent models were generated and implanted in the patient-specific aorta, from where the four metrics of performance were calculated. Results from these simulations were used to build a Gaussian process regression model for each performance metric as a function of the five design variables $c$, $p$, $t$, $w$, and $R_d$. The accuracy of the models was evaluated by the leave-one-out technique and calculating the $R^2_{pred}$ and RSME. Then, the TAVI stent optimization is posed as a multi-objective optimization problem formulated as:

$$\begin{cases} \text{Minimize } MCS(w,t,c,p,R_d), \\ \text{Maximize } RS(w,t,c,p,R_d), \\ \text{Maximize } AA(w,t,c,p,R_d), \\ \text{Minimize } E(w,t,c,p,R_d) \end{cases}$$
$$\text{s.t.}$$
$$0.2 < w < 0.5$$
$$0.2 < t < 0.5 \qquad (6)$$
$$c = \{3,4,5\}$$
$$p = \{9,12,15\}$$
$$R_d = \{1,1.03,1.2,1.5,1.73\}$$

A non-dominated sorting genetic algorithm (NSGA-II) was utilized to find the Pareto front of best models for this problem. We used a population size of 50 and 2000 generations. A uniform crossover was applied to 80%, and a one-bit mutation was applied to 20% of the population. The stop criterion was the maximum number of generations.

Five optimal designs were selected from the 50 non-dominated optimal solutions (Pareto front) to evaluate the optimization framework's results and compare them with the reference implanted device in the patient-specific geometry. One design was chosen from the center of the Pareto front. Two designs were selected from the Pareto front that were not dominated by the reference device in any of the objective functions. For selecting the other two optimal designs, a margin of safety was defined for each metric, and two designs associated with the largest margin of safety were considered as the optimal designs. The margin of safety of a model is defined by:

$$MS_{MCS}(x) = 1 \quad \frac{MCS\,(x)}{0.1} \qquad (7)$$

$$MS_{RS}(x) = \frac{RS\,(x)}{RS_{max}} \tag{8}$$

$$MS_{AA}(x) = \frac{AA\,(x)}{AA_{max}} \tag{9}$$

$$MS_{E}(x) = 1 \quad \frac{E\,(x)}{E_{max}} \tag{10}$$

$$MS(x) = \min\ (MS_{MCS}(x), MS_{RS}(x), MS_{AA}(x), MS_{E}(x)) \tag{11}$$

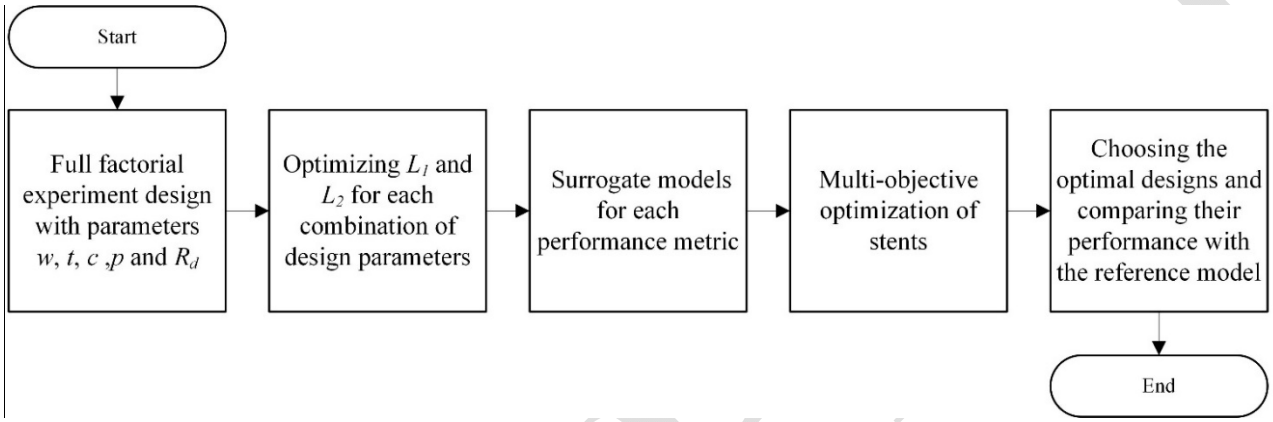


**Fig. 5.** The flowchart explaining the process of optimization framework in this study

## 2.4 The optimum versus reference device

To have a more comprehensive evaluation of the performance of the optimized devices in this specific aortic root configuration, three additional aspects associated with the device performance were evaluated and compared with the reference model: i) para-valvular leakage, ii) maximum contact pressure, and iii) maximum stress on the aortic wall. Different approaches have been proposed for evaluating the post-TAVI para-valvular leakage (PVL) in the literature [12,13,18,40]. In this study, we created a MATLAB code for assessing the gap area between the stent and the arterial wall in evenly-spaced cross-sections parallel to the annulus. Based on the approach presented by Tanaka et al. [40], the minimal gap area can be associated with the amount and the level of the post-TAVI PVL. Fig. 6c-e shows the results of this process for one of the cases of this study.

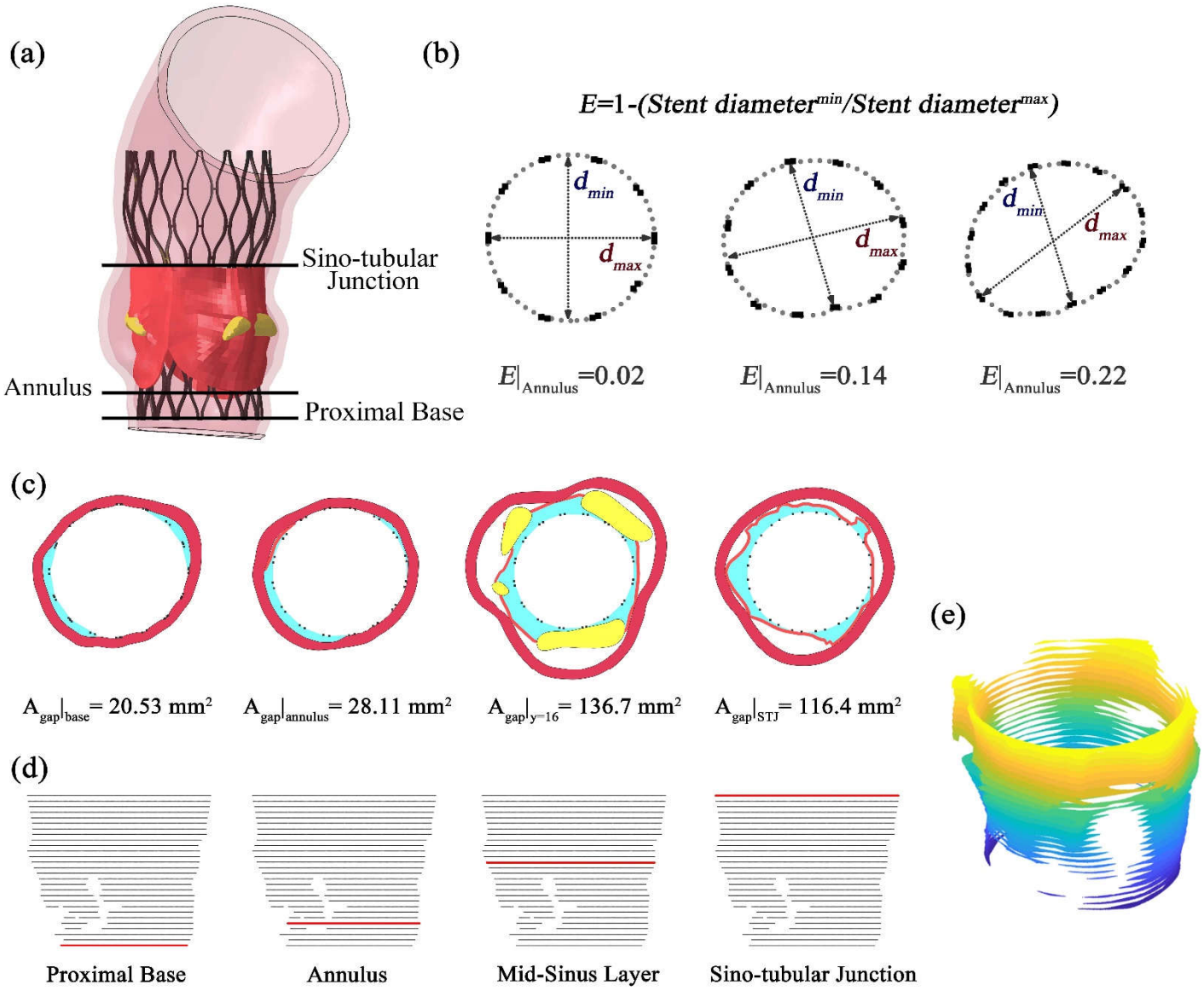


**Fig. 6.** a) The implanted configuration of all sample cases was evaluated by evenly-spaced cross-sections. b) Eccentricity of the stent after implantation is measured at the annulus plane. Samples of eccentricity measurements and the corresponding minimum and maximum diameter in the annulus area are depicted. The worst and best cases of Eccentricity in the annulus area for sample cases are 0.22 and 0.02, respectively. c) The cross-section of the aortic root after implantation is evaluated by a Matlab code, and the gap area between the device and the aortic root is measured at each level (gap area depicted in cyan). d) The side view of the gap areas. Each red line is associated with one of the layers in section c. e) The gap area for all levels of cross-sections is used to construct a 3D representation of the gap between the device and aortic root in the region between the proximal base and the sino-tubular junction.

Conduction abnormalities may occur after TAVI implantation in some cases, which may require the implantation of a permanent pacemaker. The maximum contact pressure under the area between NCC and RCC has been correlated to the probability of this complication to occur [11]. Additionally, vessel injuries happen due to the excessive stress exerted on the arterial wall [41]. Hence, the maximum stress on the aortic wall after stent deployment was calculated and reported. These three additional metrics were monitored especially for designs with high radial force to minimize the risk of tissue damage.

### 2.5 Statistical analysis

Statistical analyses were performed in Origin (OriginLab Corporation, Northampton, MA, USA). The effect of diameter profiles on the performance metrics was evaluated for each objective function. The statistical significance of the difference between these profiles was tested with a Mann-Whitney analysis in which a p-value of less than 0.05 determined significance.

## 3 Results

### 3.1 Performance Measures

The surrogate models were used for calculating the objective functions in the NSGA-II optimization. Fig.7 depicts the relationship between the calculated and the predicted response functions showing an excellent fit of the model.

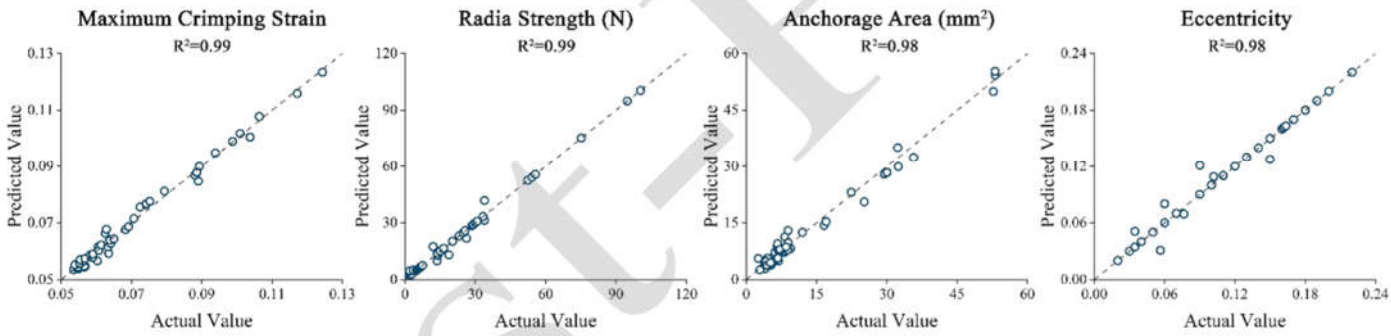


**Fig. 7.** Surrogate model validation for the objective functions; leave-one-out plots of the DOE sample cases.

These surrogates were also used to perform a sensitivity analysis of each design parameter on the performance metrics. Fig. 8 shows the result of the sensitivity analysis.

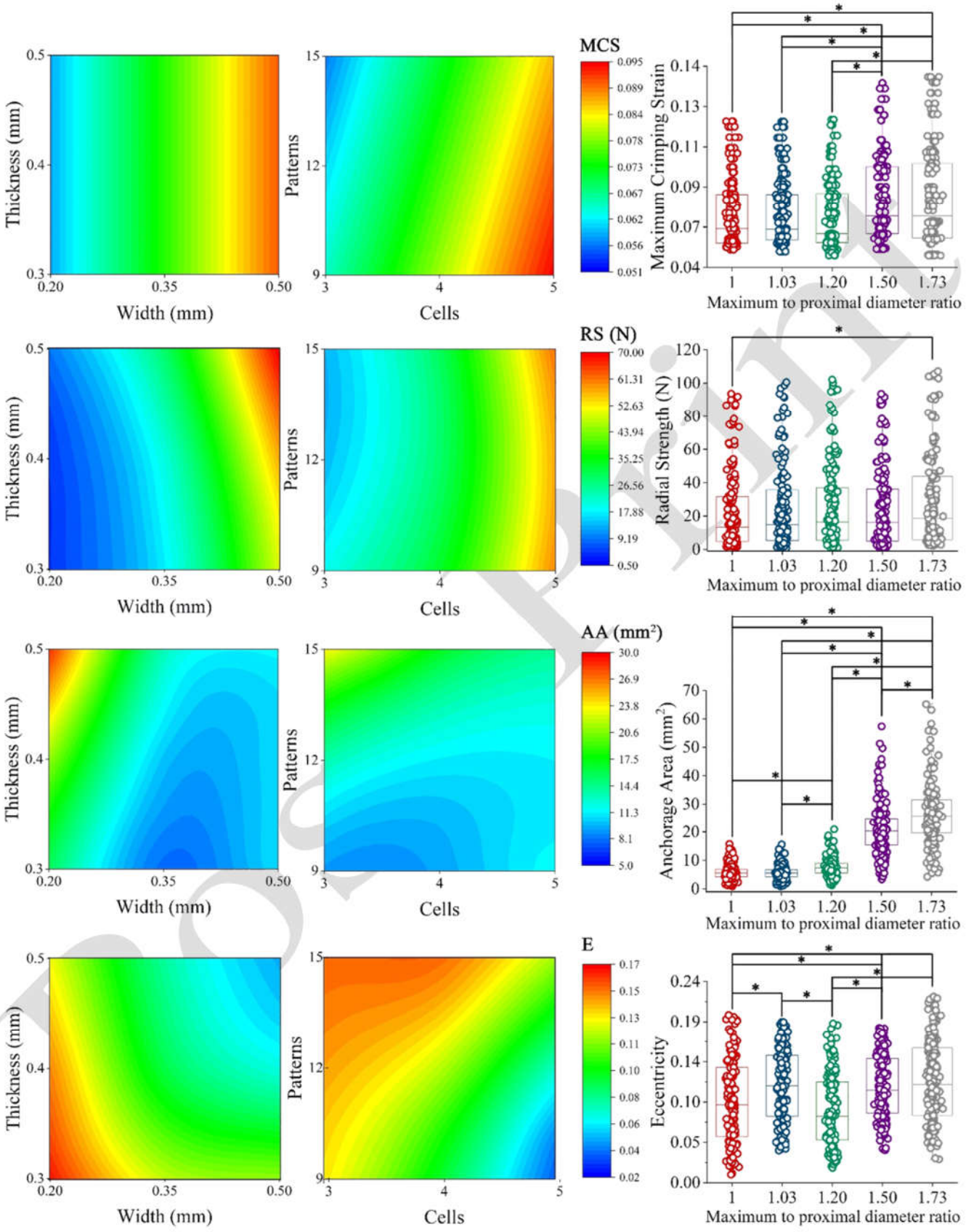


**Fig. 8.** The relationship between performance measures and the design parameters for the full factorial combination of the design parameters, using the surrogate models. The pairs with significant difference are marked with an asterisk.

The maximum strain in the stent during crimping, MCS, increased with the strut width and the number of cells while decreasing slightly with the number of patterns and being insensitive to changes in strut thickness. These results are in agreement with our previous study [21]. Different diameter profiles also affect the value of MCS. Profiles with higher maximum to proximal diameter ratios resulted in higher crimping strains. The statistical analysis shows a significant difference between two groups of diameter profiles, with diameter ratios smaller and bigger than 1.2 (p-value < 0.05). However, the difference inside these two groups was not significant (p-value > 0.05). Showing that the changes in the diameter profile don't change the maximum crimping strain up to a certain diameter ratio (profiles 1,2, and 3), but when this ratio is exceeded, the crimping strain increases to another level (profiles 4 and 5).

Regarding the radial strength of the stent, RS, the number of cells, and strut width have the most significant impact on this performance metric, with strut thickness modulating RS only at large values of strut width. In this regard, increasing strut width, strut thickness, or the number of cells increases the radial strength of the stent, consistent with previous studies [42]. On the contrary, the number of patterns and diameter profile has no effect on the radial strength for $R_d$ values associated with commercially available stents. The statistical analysis showed that only the radial strength associated with diameter profiles 1 (a cylindrical stent) and 5 were significantly different. The radial strength for the different diameter profiles was found to be in the range reported in literature for the corresponding commercial TAVI stents [23]. Despite the diameter profile not affecting the radial strength, it affects how the radial force varies with stent diameter. The shape of the radial force-diameter curve is mainly affected by the number of cells and the diameter profile of the stent. For cases with a smaller number of cells, the curve is more linear than in cases with a higher number of cells where the struts work more in bending when the stent is crimped to smaller diameters (results not shown). In general, the shape of radial force-diameter curves was consistent with previous studies [21,42].

The most important design parameter affecting the anchorage area, AA, is the diameter profile of the stent. The Mann-Whitney test showed significant differences in the anchorage area results associated with all pairs of diameter profiles, except for profiles 1 and 2, which have similar diameter ratios. Stents with a wider distal

diameter may have up to a five-fold increase in the anchorage area with respect to stents with a cylindrical form of the same size, with AA rapidly increasing for $R_d > 1.2$ (Fig. 8). The dependence of AA in other design variables is found to be rather nonlinear. In this regard, increasing strut thickness while reducing the strut width increases AA. Similarly, increasing the number of patterns and reducing the number of cells increases AA. These results are in agreement with the results of Rocatello et al., who also reported that the stents with larger diameters and large cells, i.e., lower number of cells, have better anchorage in the aortic root [19].

The eccentricity is an important factor for predicting the device performance and coaptation quality [24]. Stents with smaller strut width and thickness, a smaller number of cells, and a larger number of patterns had a more elliptic shape after implantation. The statistical analysis shows a significant difference between the effects of diameter profiles on the stent eccentricity in the annulus.

## 3.2 Optimal designs

In a multi-objective optimization problem, choosing an optimal solution is not straightforward and usually results in a trade-off evaluation of the different objective functions involved in the problem. To have a better understanding of the necessity of performing a trade-off between the four metrics of performance, five models were chosen from the Pareto front to compare against the reference device, namely: two solutions, PS1 and PS2, with the largest margin of safety as computed from Eq. 11; two solutions, PS3 and PS4, that outperformed the reference device in all performance markers; and one solution, PS5, from the middle of the Pareto front. Table 4 gives the value of the design variables and diameter profile for the selected optimal designs (the reference stent is reported for completeness)

**Table 4.** Value of design variables for the reference stent and the five optimal solutions

| **Design** | ***c*** | ***p*** | ***t*** (mm) | ***w*** (mm) | $L_1$ (mm) | $L_2$ (mm) | $R_d$ |
|---|---|---|---|---|---|---|---|
| Reference | 5 | 15 | 0.20 | 0.30 | 8.58 | 7.38 | 1.20 |
| PS1 | 3 | 15 | 0.50 | 0.47 | 15.0 | 15.0 | 1.73 |
| PS2 | 3 | 15 | 0.50 | 0.50 | 16.7 | 14.2 | 1.20 |
| PS3 | 4 | 15 | 0.50 | 0.46 | 12.5 | 11.7 | 1.20 |
| PS4 | 3 | 9 | 0.50 | 0.50 | 15.2 | 15.2 | 1.73 |
| PS5 | 5 | 15 | 0.40 | 0.35 | 10.0 | 10.0 | 1 |

Fig. 9 shows the trade-off graphs of the objective functions for the different Pareto solutions, the selected optimal models, and the reference device.

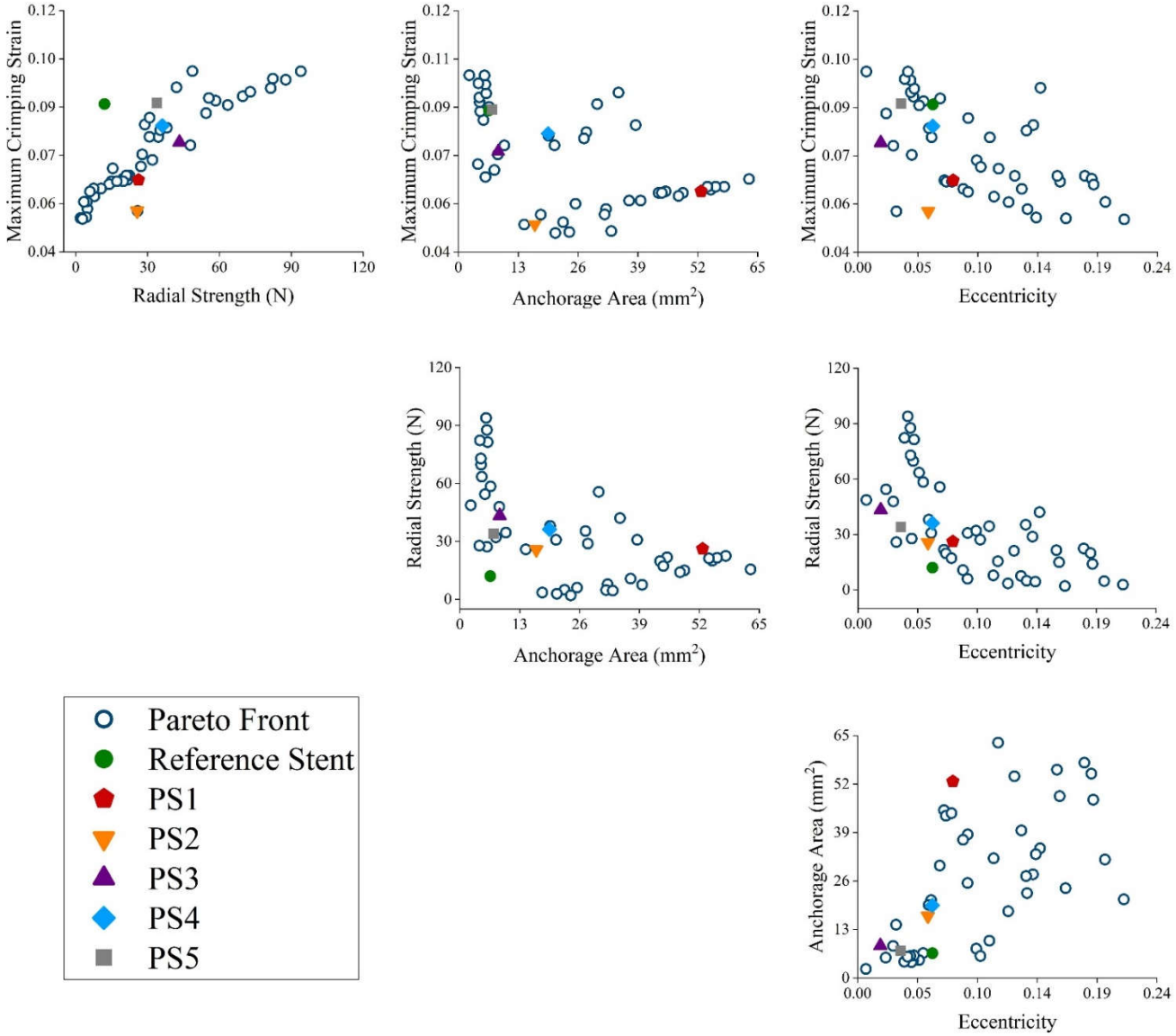


**Fig. 9.** Trade-off graphs of four objective functions

Published manuscript at https://doi.org/10.1016/j.cmpb.2022.106912

The trade-off graphs show that the maximum crimping strain and radial strength have a monotonic relationship. This means increasing the radial strength happens at the cost of increasing the maximum crimping strain. The increase in anchorage area is in favor of decreasing the crimping strain. Moreover, the results in Fig. 9 indicate that increasing radial stiffness reduces the eccentricity at the annulus, also observed in Fig.8 .In general, the pairs of radial strength-eccentricity and crimping strain-anchorage area objective functions change in favor of each other and result in an undesirable change in the other pair of objective functions. Hence, choosing the optimal device should be performed depending on the patient's physiological needs.

All five models were implanted in the patient's model aorta, and the four performance metrics were calculated. Further, additional performance metrics: the minimal gap area (MGA), the maximum contact pressure (CP), and maximum stress in the arterial wall (MAS), were computed. Results for all six models are shown in Fig. 10a in the form of a radar plot. The value of the performance indices has been normalized to vary in the range from zero to one, with the larger the value, the better. Hence, models with a larger area in the radar plot indicate better performance in the implantation.

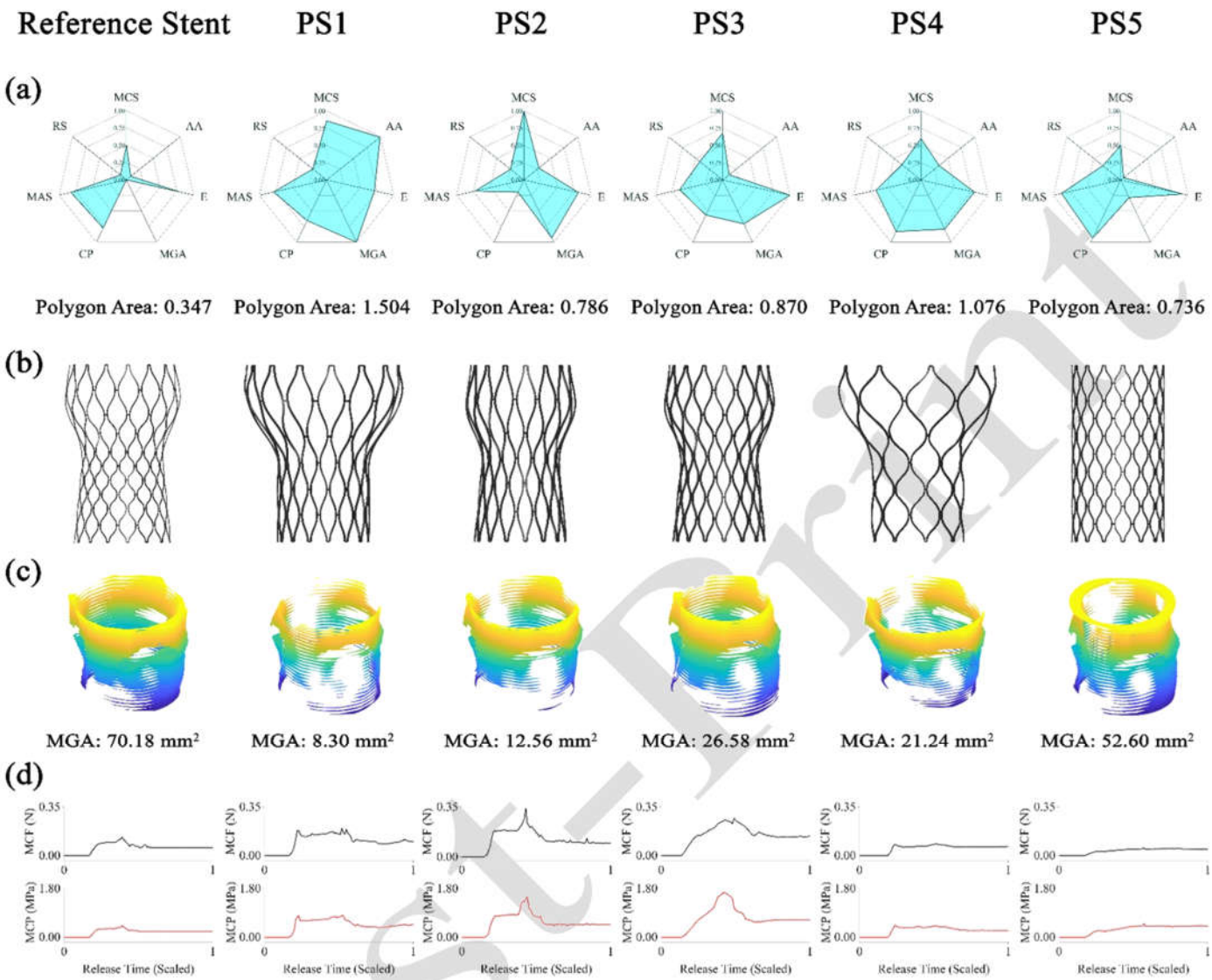


**Fig. 10.** The comparison of performance measures of the implanted reference device and the selected optimal solutions. a) The radar plots represent the performance of each device. The larger the area of the polygon, the better the performance. b) The stent configuration of the reference model and the optimal solutions. c) MGA: minimal gap area between the stent and the aortic root. d) The "maximum contact force (MCF) versus time" for the proximal base of the stent and the "maximum contact pressure (MCP) versus time" for the aortic wall in the LVOT region. It is to be noted that the CP in the radar plots is associated with the maximum contact pressure in the region under the area between the non-coronary cusp (NCC) and right coronary cusp (RCC). Still, the MCP represents the maximum contact pressure in all regions of the LVOT.

The radar plot shows the general improvement in objective functions for the different optimal designs. The optimal devices show up to a 40% decrease in the maximum crimping strain, 261% increase in the radial strength, 67% reduction in the eccentricity at the annulus, and about an 8-fold rise in the anchorage area compared to the

reference device. All optimal models have better performance than the reference model in the minimal gap area. However, the reference model shows a similar performance regarding the contact pressure, CP, and the maximum stress exerted on the aortic root, MAS. However, these values are very much comparable among all optimized models except for PS2, which shows a significantly larger contact pressure as compared to the other devices. Further, comparing the areas in the radar plot suggest that optimal designs favor stents with larger $R_d$. Fig. 10d shows the maximum contact force at the proximal base of the stent (MCF) and the maximum contact pressure exerted on the LVOT (MCP) change during the release procedure. In the initial phase of release (20%- 50% of release progress), the proximal base of the prosthesis is in contact with the LVOT while the distal portion is still in the catheter. During this phase, the proximal diameter of the stent increases gradually, increasing the MCF and MCP. At approximately 60% of the release time, the distal portion of the stent is released into the ascending aorta, leading to a change in the stent configuration and reducing the proximal diameter of the stent. At this point, the MCP and the MCF reduce to the post-intervention value. The results show that optimal designs PS2 and PS3, both with the same diameter profile as the reference stent, deliver a larger MCP (1.49 MPa and 1.66 MPa for PS2 and PS3, respectively, versus 0.43 MPa for the reference stent) and MCF (0.34 N and 0.27 N for PS2 and PS3 versus 0.13 N for the reference stent) during the release phase and provide a larger post-intervention MCP (0.48 MPa and 0.65 MPa for PS2 and PS3 versus 0.21 MPa for the reference stent) and MCF (0.10 N and 0.14 N for PS2 and PS3 versus 0.06 N for the reference stent). On the contrary, design PS1 and PS4 with a different diameter profile show similar values of MCP and MCF as the reference stent, particularly design PS4 with differences of less than 10%.

# 4 Discussion

In the optimization studies regarding TAVI stents, the performance measures are often conflicting, and finding the optimal design is a complex procedure with some necessary trade-offs. The maximum crimping strain and radial strength are structural metrics and can be evaluated regardless of the aortic root geometry. In contrast, other performance metrics evaluated in this study are dependent on the specific patient's geometry. Therefore, using

patient-specific geometry and including the calcifications are necessary since the shape, position, and size of the calcifications influence the final configuration of the device and its performance [15]. Therefore, identifying the optimal device for a given patient requires solving a multi-objective optimization problem on the patient's specific geometry.

To reduce the computational cost of the multi-objective optimization, surrogate models were built and used for the optimization. Also, these models allow for a comprehensive analysis of the effect of each design parameter on the different performance metrics (Fig. 8). In this regard, it was found that strut width significantly impacts most of the performance metrics. An increase in the strut width can result in an increase in the maximum crimping strain and radial strength and reduce stent eccentricity. In contrast, for most performance measures, the strut thickness has a marginal role. The increase in this parameter leads to a rise in the radial strength while decreasing the stent eccentricity. The number of cells in a pattern is an important factor in the stent design. Stents with a larger number of cells reach a higher maximum crimping strain have larger radial strength and smaller eccentricity. On the contrary, increasing the number of patterns favors in reducing the crimping strain while slightly increasing the eccentricity of the stent. The diameter profile of the stents affects the maximum crimping strain, the shape of the radial force-displacement curve, and the anchorage area. Stents with a larger maximum diameter to proximal diameter ratio have a better anchorage in the aortic root, but they also have slightly larger crimping strain.

The optimized models outperformed the reference device in most of the performance metrics. Model PS2, which has the same diameter profile, Profile 3, and the same number of patterns, 15, but a different number of cells (three instead of the five), has the smallest maximum crimping strain. Reducing the number of cells from 5 to 3 has had a critical role in this change (about a 40% decrease). Model PS3, which has the same diameter profile and number of patterns as the reference model and the PS2 design, with four cells, has a maximum crimping strain between that of PS1 and PS2 while having the smallest eccentricity among the models (0.02). Schuhbaeck et al. [43] evaluated the pre-and post-operative eccentricity of the patients receiving self-expandable (CoreValve) and balloon-expandable (Edwards Sapien) prostheses and concluded that the eccentricity of aortic annulus for

patients with self-expandable stents was significantly larger than the balloon-expandable ones (0.15 ± 0.07 vs. 0.06 ± 0.05, $p < 0.0001$). The cut-off value for circularity of the prosthesis in the annulus is set to 0.1, and eccentricity values larger than 0.1 are associated with incomplete expansion and valve malfunction [9]. All the optimal samples have eccentricities smaller than the cut-off value. Aside from the design of the stents, the relatively smaller size of the calcification in this patient's aortic root compared to the mentioned study (553.73 $mm^3$ vs. 571.6 ± 410.9 $mm^3$) can be an influential factor on the small amounts of the eccentricity. The PS1 and PS4 models have the same diameter profile, the number of cells, and a slightly different strut cross-section; however, the anchorage area of the PS1 design with 15 patterns is about 2.7 times larger than that of the PS4 design with nine pattern repetitions.

The contact pressure in PS1 is 83% larger than the contact pressure in the PS4 with a smaller number of patterns. This is in accordance with the results of Rocatello et al., indicating models with larger first cells exert smaller amounts of contact pressure on the LVOT [19]. The Pareto front evaluation shows the most repeated configurations are the ones with three cells, 15 patterns, and the diameter profile 5. This combination has resulted in models with smaller radial force with respect to other models in the design space. However, for the case of PS1, the desirable amounts of anchorage area, the minimal gap area and eccentricity show that the device has been able to open the calcified diseased valve and provide a good apposition to the aortic root. Models PS3 and PS5 with higher radial forces between the optimal designs have shown smaller eccentricity which is consistent with the results of Finotello et al. [12], indicating that the models with larger radial strength are more successful in pushing the calcium blocks outwards. The PS3 design, on the other hand, has exerted the largest amount of stress on the aortic wall. However, this stress does not exceed the threshold of 2.5MPa indicated by Wang et al. [41]. Model PS2 has an acceptable performance in maximum crimping strain, eccentricity, minimal gap area, and the maximum stress exerted on the aorta; however, the contact pressure is relatively high (0.48 MPa). The cut-off value of the contact pressure for indicating the high risk of conductions abnormalities is different for various stent models. Rocatello et al. introduced the 0.39 MPa for the CoreValve devices [11] and the 0.36 MPa for Lotus

devices [44]. Even though the stent designs and the simulation set-up are not the same, these marginal amounts of contact pressure can hint at the probability of the conduction abnormalities.

The final position of the prosthetic valve within the aortic root strongly influences the procedural outcome. While positioning the valve too high with respect to the annulus may cause paravalvular aortic regurgitation, positioning the valve too low might increase the risk of post-intervention conduction abnormalities [45]. Hence, from a procedural viewpoint, the valve needs to remain in the primary position during the implantation to prevent the valve from diving deeper into the left ventricle, increasing the risk of post-intervention conduction abnormalities. In this regard, the large contact force delivered by designs PS2 and PS3 during the initial release phase while providing an adequate contact pressure after full deployment may suffice to reduce the risk of conduction abnormalities post-intervention.

In general, each patient has specific anatomic and physiologic needs. The optimal designs should be evaluated and chosen based on these requirements. The framework presented in this study explores the design space and, while evaluating the effect of each design parameter on different performance metrics, provides a collection of optimal devices to choose from. As mentioned in the results section, these metrics can change in favor of improving or at the cost of worsening each other, and what guides the optimization is a combination of these trade-offs. Increasing the fatigue life of the stent and the conformability of the stent to the aortic root is possible at the cost of reducing the ability to push calcifications and keeping the annulus circular. The decision-making on the optimal design depends on deciding the most important factors coupled with the needs and requirements of each patient.

The result of this study should be perceived considering some limitations. The fluid simulation and the device's performance in the cardiovascular cycle are not evaluated. The gap area assessed in this study is a purely geometric estimation of the PVL, which can be less accurate [18] than the fluid-structure interaction simulations in which a more accurate investigation of the PVL is possible [15]. The material properties of the stent frame are not the same for all manufacturing companies, and these properties can change the optimization results. In this study, we used the same NiTi properties for all cases. The geometric model of the aorta represents the end-

diastolic configuration and therefore corresponds to a pressurized configuration. However, the computations performed on the patient-specific geometry have neglected the pre-stress field. In addition, we used only one patient-specific geometry for the optimization study. Although the framework can be used for other generic or patient-specific aortic root geometries, the reported optimal designs are optimal in this specific geometry and should not be considered generally optimal designs. The different aortic root geometry, size, and position of the calcified deposits in each individual can change the stent's performance metrics, and selecting the optimal design will reflect the particular requirements of the patients' condition. This framework can be coupled with pre-operative imaging to have a more accurate design, fitting each patient's needs and enhancing the device's performance. Last but not least, the framework has been applied to a single patient geometry, and therefore the results are optimal for this specific geometry. However, the framework can be adapted to multiple patient-specific aortic root configurations, leading to a more comprehensive performance evaluation, optimization, and finding clinically feasible solutions. It is necessary to mention that this optimization framework is based on the mechanical performance of the TAVI device in terms of radial stiffness, maximum strain, eccentricity, and anchorage area, among other metrics. This corresponds to the first step toward an improved design of new TAVI stents. A more comprehensive design optimization strategy should consider evaluating and improving the clinical outcome of the valve. This could be achieved by considering the simulation of different valve implantation scenarios from which these specific clinical outcome metrics can be evaluated. However, the multi-objective characteristic of the proposed optimization framework allows for easy consideration of new metrics, i.e., clinical outcome, in the design pipeline. Future work will consider the effect of material properties of the aorta, leaflets, and calcifications to evaluate the robustness of the results in front of the uncertainty in patients' specific tissue behavior. In addition, Future works will consider the pre-stress associated with the diastolic pressure to replicate the real end-diastole configurations of patients.

In this study, an optimization framework for the TAVI stent design was proposed. The framework was designed to optimize the overall shape of the stent, strut cross-section, the number of repeating cells and patterns, and the size of the cells in consecutive steps. The objective functions include the TAVI stents' structural and functional

performance measures. The maximum strain during stent crimping, the radial strength, the anchorage area, and the stent eccentricity at the annulus level were investigated to find patient-specific optimal designs. Regression surrogate models were utilized to evaluate each design parameter's effect on the objective function and perform the NSGA-II optimization. The optimal designs were compared with the implanted device more thoroughly and confirmed the improvement provided by the optimization framework. The results suggest that prostheses with a maximum to proximal diameter ratio larger than 1.2 outperform those with a more cylindrical shape when working with calcified valves. Since the stents with a larger distal area provide a larger anchorage area while reducing contact pressure and minimizing regurgitation. The proposed framework reduces the computational cost of transcatheter valve stent optimization. It can be used for different patient-specific aortic root geometries to optimize the design and manufacturing process of the TAVI frames and help the process of decision-making prior to the TAVI.

# 5 Acknowledgments

Giulia Luraghi, Lorenza Petrini, Francesco Migliavacca, and Josè Felix Rodriguez Matas are supported by a grant by the Italian Ministry of Education, University and Research (Grant number 1613 FISR2019_03221, CECOMES).

**Declaration of Competing Interest**

The authors declare that they have no known competing financial interests or personal relationships that could have appeared to influence the work reported in this paper.

**CRediT author statement**

**Sara Barati:** Conceptualization, Methodology, Software, Investigation, Formal analysis, Writing - Original Draft, Review & Editing; **Nasser Fatouraee:** Supervision, Project administration; **Malikeh Nabaei:** Writing - Review & Editing; **Lorenza Petrini:** Writing - Review & Editing; **Francesco Migliavacca:** Project administration, Writing - Review & Editing; **Giulia Luraghi:** Conceptualization, Methodology , Writing -

Review & Editing; **Josè Felix Rodriguez Matas:** Project administration, Conceptualization, Methodology, Validation, Writing - Review & Editing.

## References

[1] A. Sedrakyan, S.S. Dhruva, J. Shuhaiber, Transcatheter Aortic Valve Replacement in Younger Individuals, JAMA Intern. Med. 177 (2017) 159. https://doi.org/10.1001/jamainternmed.2016.8104.

[2] J.J. Popma, G. Michael Deeb, S.J. Yakubov, M. Mumtaz, H. Gada, D. O'Hair, T. Bajwa, J.C. Heiser, W. Merhi, N.S. Kleiman, J. Askew, P. Sorajja, J. Rovin, S.J. Chetcuti, D.H. Adams, P.S. Teirstein, G.L. Zorn, J.K. Forrest, D. Tchétché, J. Resar, A. Walton, N. Piazza, B. Ramlawi, N. Robinson, G. Petrossian, T.G. Gleason, J.K. Oh, M.J. Boulware, H. Qiao, A.S. Mugglin, M.J. Reardon, Transcatheter aortic-valve replacement with a self-expanding valve in low-risk patients, N. Engl. J. Med. 380 (2019) 1706–1715. https://doi.org/10.1056/NEJMoa1816885.

[3] L.P. Dasi, H. Hatoum, A. Kheradvar, R. Zareian, S.H. Alavi, W. Sun, C. Martin, T. Pham, Q. Wang, P.A. Midha, V. Raghav, A.P. Yoganathan, On the Mechanics of Transcatheter Aortic Valve Replacement, Ann. Biomed. Eng. 45 (2017) 310–331. https://doi.org/10.1007/s10439-016-1759-3.

[4] O.M. Rotman, M. Bianchi, R.P. Ghosh, B. Kovarovic, O.M. Rotman, M. Bianchi, R.P. Ghosh, B. Kovarovic, D. Bluestein, Principles of TAVR valve design, modelling, and testing, Expert Rev. Med. Devices. 15 (2018) 771–791. https://doi.org/10.1080/17434440.2018.1536427.

[5] M.J. Reardon, N.M. Van Mieghem, J.J. Popma, N.S. Kleiman, L. Søndergaard, M. Mumtaz, D.H. Adams, G.M. Deeb, B. Maini, H. Gada, S. Chetcuti, T. Gleason, J. Heiser, R. Lange, W. Merhi, J.K. Oh, P.S. Olsen, N. Piazza, M. Williams, S. Windecker, S.J. Yakubov, E. Grube, R. Makkar, J.S. Lee, J. Conte, E. Vang, H. Nguyen, Y. Chang, A.S. Mugglin, P.W.J.C. Serruys, A.P. Kappetein, Surgical or Transcatheter Aortic-Valve Replacement in Intermediate-Risk Patients, N. Engl. J. Med. 376 (2017) 1321–1331. https://doi.org/10.1056/nejmoa1700456.

[6] G. Athappan, E. Patvardhan, E.M. Tuzcu, L.G. Svensson, P.A. Lemos, C. Fraccaro, G. Tarantini, J.M.

Sinning, G. Nickenig, D. Capodanno, C. Tamburino, A. Latib, A. Colombo, S.R. Kapadia, Incidence, predictors, and outcomes of aortic regurgitation after transcatheter aortic valve replacement: Meta-analysis and systematic review of literature, J. Am. Coll. Cardiol. 61 (2013) 1585–1595. https://doi.org/10.1016/j.jacc.2013.01.047.

[7] F. Campelo-Parada, L. Nombela-Franco, M. Urena, A. Regueiro, P. Jiménez-Quevedo, M. Del Trigo, C. Chamandi, T. Rodríguez-Gabella, V. Auffret, O. Abdul-Jawad Altisent, R. DeLarochellière, J.-M. Paradis, E. Dumont, F. Philippon, N. Pérez-Castellano, R. Puri, C. Macaya, J. Rodés-Cabau, Timing of Onset and Outcome of New Conduction Abnormalities Following Transcatheter Aortic Valve Implantation: Role of Balloon Aortic Valvuloplasty, Rev. Española Cardiol. (English Ed. 71 (2018) 162–169. https://doi.org/10.1016/j.rec.2017.04.010.

[8] G.Y. Perlman, P. Blanke, D. Dvir, G. Pache, T. Modine, M. Barbanti, E.W. Holy, H. Treede, P. Ruile, F.J. Neumann, C. Gandolfo, F. Saia, C. Tamburino, G. Mak, C. Thompson, D. Wood, J. Leipsic, J.G. Webb, Bicuspid Aortic Valve Stenosis: Favorable Early Outcomes with a Next-Generation Transcatheter Heart Valve in a Multicenter Study, JACC Cardiovasc. Interv. 9 (2016) 817–824. https://doi.org/10.1016/j.jcin.2016.01.002.

[9] S. Morganti, N. Brambilla, A.S. Petronio, A. Reali, F. Bedogni, F. Auricchio, Prediction of patient-specific post-operative outcomes of TAVI procedure: The impact of the positioning strategy on valve performance, J. Biomech. 49 (2016) 2513–2519. https://doi.org/10.1016/j.jbiomech.2015.10.048.

[10] M. Bianchi, G. Marom, R.P. Ghosh, O.M. Rotman, P. Parikh, L. Gruberg, D. Bluestein, Patient-specific simulation of transcatheter aortic valve replacement: impact of deployment options on paravalvular leakage, Biomech. Model. Mechanobiol. 18 (2019) 435–451. https://doi.org/10.1007/s10237-018-1094-8.

[11] G. Rocatello, N. El Faquir, G. De Santis, F. Iannaccone, J. Bosmans, O. De Backer, L. Sondergaard, P. Segers, M. De Beule, P. De Jaegere, P. Mortier, Patient-Specific Computer Simulation to Elucidate the Role of Contact Pressure in the Development of New Conduction Abnormalities after Catheter-Based Implantation of a Self-Expanding Aortic Valve, Circ. Cardiovasc. Interv. 11 (2018) 1–9.

https://doi.org/10.1161/CIRCINTERVENTIONS.117.005344.

[12] A. Finotello, R.M. Romarowski, R. Gorla, G. Bianchi, F. Bedogni, F. Auricchio, S. Morganti, Performance of high conformability vs. high radial force devices in the virtual treatment of TAVI patients with bicuspid aortic valve, Med. Eng. Phys. 89 (2021) 42–50. https://doi.org/10.1016/j.medengphy.2021.02.004.

[13] B. Bosmans, N. Famaey, E. Verhoelst, J. Bosmans, J. Vander Sloten, A validated methodology for patient specific computational modeling of self-expandable transcatheter aortic valve implantation, J. Biomech. 49 (2016) 2824–2830. https://doi.org/10.1016/j.jbiomech.2016.06.024.

[14] W. Mao, Q. Wang, S. Kodali, W. Sun, P.A. Root, Numerical Parametric Study of Paravalvular Leak Following a Transcatheter Aortic Valve Deployment into a Patient-Specific Aortic Root, J. Biomech. Eng. 140 (2018) 1–11. https://doi.org/10.1115/1.4040457.

[15] G. Luraghi, F. Migliavacca, A. García-González, C. Chiastra, A. Rossi, D. Cao, G. Stefanini, J.F. Rodriguez Matas, On the Modeling of Patient-Specific Transcatheter Aortic Valve Replacement: A Fluid–Structure Interaction Approach, Cardiovasc. Eng. Technol. 10 (2019) 437–455. https://doi.org/10.1007/s13239-019-00427-0.

[16] R.P. Ghosh, G. Marom, M. Bianchi, K. D'souza, W. Zietak, D. Bluestein, Numerical evaluation of transcatheter aortic valve performance during heart beating and its post-deployment fluid–structure interaction analysis, Biomech. Model. Mechanobiol. 19 (2020) 1725–1740. https://doi.org/10.1007/s10237-020-01304-9.

[17] G. Luraghi, J.F.R. Matas, M. Beretta, N. Chiozzi, L. Iannetti, F. Migliavacca, The impact of calcification patterns in transcatheter aortic valve performance: a fluid-structure interaction analysis, Comput. Methods Biomech. Biomed. Engin. 0 (2020) 1–9. https://doi.org/10.1080/10255842.2020.1817409.

[18] G.M. Bosi, C. Capelli, M.H. Cheang, N. Delahunty, M. Mullen, A.M. Taylor, S. Schievano, Population-specific material properties of the implantation site for transcatheter aortic valve replacement finite element simulations, J. Biomech. 71 (2018) 236–244. https://doi.org/10.1016/j.jbiomech.2018.02.017.

[19] G. Rocatello, G. De Santis, S. De Bock, M. De Beule, P. Segers, P. Mortier, Optimization of a

Transcatheter Heart Valve Frame Using Patient-Specific Computer Simulation, Cardiovasc. Eng. Technol. 10 (2019) 456–468. https://doi.org/10.1007/s13239-019-00420-7.

[20] D. Carbonaro, D. Gallo, U. Morbiducci, A. Audenino, C. Chiastra, In silico biomechanical design of the metal frame of transcatheter aortic valves: multi-objective shape and cross-sectional size optimization, Struct. Multidiscip. Optim. (2021) 0–3. https://doi.org/10.1007/s00158-021-02944-w.

[21] S. Barati, N. Fatouraee, M. Nabaei, F. Berti, L. Petrini, F. Migliavacca, J.F. Rodriguez Matas, A computational optimization study of a self-expandable transcatheter aortic valve, Comput. Biol. Med. 139 (2021) 104942. https://doi.org/10.1016/j.compbiomed.2021.104942.

[22] F. Sturla, M. Ronzoni, M. Vitali, A. Dimasi, R. Vismara, G. Preston-Maher, G. Burriesci, E. Votta, A. Redaelli, Impact of different aortic valve calcification patterns on the outcome of transcatheter aortic valve implantation: A finite element study, J. Biomech. 49 (2016) 2520–2530. https://doi.org/10.1016/j.jbiomech.2016.03.036.

[23] O.M. McGee, W. Sun, L.M. McNamara, An in vitro model quantifying the effect of calcification on the tissue–stent interaction in a stenosed aortic root, J. Biomech. 82 (2019) 109–115. https://doi.org/10.1016/j.jbiomech.2018.10.010.

[24] A. Finotello, S. Morganti, F. Auricchio, Finite element analysis of TAVI: Impact of native aortic root computational modeling strategies on simulation outcomes, Med. Eng. Phys. 47 (2017). https://doi.org/10.1016/j.medengphy.2017.06.045.

[25] D. Todaro, A. Picci, M. Barbanti, Technical characteristics and evidence to date for FDA-and CE Mark-approved valves, Interv. Today. 11 (2017) 53–58. https://citoday.com/pdfs/cit0317_F5_Barbanti.pdf.

[26] J. Kusneri, G. Luraghi, F. Khodaeei, J.F.L.R. Matas, F. Migliavacca, E.R. Edelman, F.R. Nezami, Understanding TAVR device expansion as it relates to morphology of the bicuspid aortic valve: A simulation study, PLoS One. 16 (2021) 1–9. https://doi.org/10.1371/journal.pone.0251579.

[27] S. Pasta, S. Cannata, G. Gentile, M. Di Giuseppe, F. Cosentino, F. Pasta, V. Agnese, D. Bellavia, G.M. Raffa, M. Pilato, C. Gandolfo, Simulation study of transcatheter heart valve implantation in patients with

stenotic bicuspid aortic valve, Med. Biol. Eng. Comput. 58 (2020) 815–829. https://doi.org/10.1007/s11517-020-02138-4.

[28] K. Cao, P. Sucosky, Computational comparison of regional stress and deformation characteristics in tricuspid and bicuspid aortic valve leaflets, Int. j. Numer. Method. Biomed. Eng. 33 (2017) 1–21. https://doi.org/10.1002/cnm.2798.

[29] S. Pfensig, S. Kaule, R. Ott, C. Wüstenhagen, M. Stiehm, J. Keiler, A. Wree, N. Grabow, K.P. Schmitz, S. Siewert, Numerical simulation of a transcatheter aortic heart valve under application-related loading, Curr. Dir. Biomed. Eng. 4 (2018) 185–189. https://doi.org/10.1515/cdbme-2018-0046.

[30] E. Dordoni, Fatigue analysis of Nitinol cardiovascular devices. PhD Thesis, Politecnico di Milano, 2014.

[31] J. Bailey, N. Curzen, N.W. Bressloff, Assessing the impact of including leaflets in the simulation of TAVI deployment into a patient-specific aortic root, Comput. Methods Biomech. Biomed. Engin. 19 (2016) 733–744. https://doi.org/10.1080/10255842.2015.1058928.

[32] A.S. Petronio, J.M. Sinning, N. Van Mieghem, G. Zucchelli, G. Nickenig, R. Bekeredjian, J. Bosmans, F. Bedogni, M. Branny, K. Stangl, J. Kovac, M. Schiltgen, S. Kraus, P. De Jaegere, Optimal implantation depth and adherence to guidelines on permanent pacing to improve the results of transcatheter aortic valve replacement with the medtronic corevalve system: The CoreValve prospective, international, post-market ADVANCE-II study, JACC Cardiovasc. Interv. 8 (2015) 837–846. https://doi.org/10.1016/j.jcin.2015.02.005.

[33] J. Mummert, E. Sirois, W. Sun, Quantification of biomechanical interaction of transcatheter aortic valve stent deployed in porcine and ovine hearts, Ann. Biomed. Eng. 41 (2013) 577–586. https://doi.org/10.1007/s10439-012-0694-1.

[34] C.J. Schultz, A. Weustink, N. Piazza, A. Otten, C. Ms, N. Mollet, G. Krestin, R.J. Van Geuns, P. De Feyter, P.W.J. Serruys, P. De Jaegere, Geometry and Degree of Apposition of the CoreValve ReValving System With Multislice Computed Tomography After Implantation in Patients With Aortic Stenosis, JAC. 54 (2009) 911–918. https://doi.org/10.1016/j.jacc.2009.04.075.

[35] L. Petrini, W. Wu, E. Dordoni, A. Meoli, F. Migliavacca, G. Pennati, Fatigue behavior characterization of nitinol for peripheral stents, Funct. Mater. Lett. 5 (2012). https://doi.org/10.1142/S1793604712500129.

[36] L. Petrini, A. Bertini, F. Berti, G. Pennati, F. Migliavacca, The role of inelastic deformations in the mechanical response of endovascular shape memory alloy devices, Proc. Inst. Mech. Eng. Part H J. Eng. Med. 231 (2017) 391–404. https://doi.org/10.1177/0954411917696336.

[37] N.S. Ribeiro, J. Folgado, H.C. Rodrigues, Surrogate-based visualization and sensitivity analysis of coronary stent performance: A study on the influence of geometric design, Int. j. Numer. Method. Biomed. Eng. 34 (2018) 1–28. https://doi.org/10.1002/cnm.3125.

[38] ASTM F3067-14, Guide for Radial Loading of Balloon Expandable and Self Expanding, (2014). https://doi.org/10.1520/F3067.

[39] R. Gorla, M. Casenghi, A. Finotello, F. De Marco, S. Morganti, D. Regazzoli, G. Bianchi, E. Acerbi, A. Popolo Rubbio, N. Brambilla, L. Testa, F. Castriota, F. Auricchio, B. Reimers, F. Bedogni, Outcome of transcatheter aortic valve replacement in bicuspid aortic valve stenosis with new-generation devices, Interact. Cardiovasc. Thorac. Surg. 32 (2021) 20–28. https://doi.org/10.1093/icvts/ivaa231.

[40] Y. Tanaka, S. Saito, S. Sasuga, A. Takahashi, Y. Aoyama, K. Obama, M. Umezu, K. Iwasaki, Quantitative assessment of paravalvular leakage after transcatheter aortic valve replacement using a patient-specific pulsatile flow model, Int. J. Cardiol. 258 (2018) 313–320. https://doi.org/10.1016/j.ijcard.2017.11.106.

[41] Q. Wang, S. Kodali, C. Primiano, W. Sun, Simulations of transcatheter aortic valve implantation : implications for aortic root rupture, Biomech. Model. Mechanobiol. 14 (2014) 29–38. https://doi.org/10.1007/s10237-014-0583-7.

[42] M.S. Cabrera, C.W.J. Oomens, F.P.T. Baaijens, Understanding the requirements of self-expandable stents for heart valve replacement: Radial force, hoop force and equilibrium, J. Mech. Behav. Biomed. Mater. 68 (2017) 252–264. https://doi.org/10.1016/j.jmbbm.2017.02.006.

[43] A. Schuhbaeck, C. Weingartner, M. Arnold, J. Schmid, T. Pflederer, M. Marwan, J. Rixe, H. Nef, C. Schneider, M. Lell, M. Uder, S. Ensminger, R. Feyrer, M. Weyand, S. Achenbach, Aortic annulus

eccentricity before and after transcatheter aortic valve implantation: Comparison of balloon-expandable and self-expanding prostheses, Eur. J. Radiol. 84 (2015) 1242–1248. https://doi.org/10.1016/j.ejrad.2015.04.003.

[44] G. Rocatello, N. El Faquir, O. de Backer, M.J. Swaans, A. Latib, L. Vicentini, P. Segers, M. De Beule, P. de Jaegere, P. Mortier, The Impact of Size and Position of a Mechanical Expandable Transcatheter Aortic Valve: Novel Insights Through Computational Modelling and Simulation, J. Cardiovasc. Transl. Res. 12 (2019) 435–446. https://doi.org/10.1007/s12265-019-09877-2.

[45] R.M.A. Van Der Boon, P. Houthuizen, M. Urena, T.T. Poels, N.M. Van Mieghem, G.R.G. Brueren, S. Altintas, R.J. Nuis, P.W. Serruys, L.A.F.M. Van Garsse, R.T. Van Domburg, J.R. Cabau, P.P.T. De Jaegere, F.W. Prinzen, Trends in the occurrence of new conduction abnormalities after transcatheter aortic valve implantation, Catheter. Cardiovasc. Interv. 85 (2015) 144–152. https://doi.org/10.1002/ccd.25765.